Research Square

Preprints are preliminary reports that have not undergone peer review.
They should not be considered conclusive, used to inform clinical practice,
or referenced by the media as validated information.

Interior geometry reconstructs the sarcophagus envelope and exterior slope of the Great Pyramid of Khufu

Lucas Giovani Ribeiro

coin26@mail.com

Independent Researcher

MARCOS ANDRÉ SIMONSSINI

Independent Researcher

Article

Keywords:

Posted Date: November 11th, 2026

DOI: https://doi.org/10.21203/rs.3.rs-11530919/v1

License: This work is licensed under a Creative Commons Attribution 4.0 International License.
Read Full License

Additional Declarations: No competing interests reported.

Interior geometry reconstructs the sarcophagus envelope and exterior slope of the Great Pyramid of Khufu

Lucas Giovani Ribeiro[1]*

ORCID: https://orcid.org/0009-0002-1417-0062

Marcos André Simonssini[1]

ORCID: https://orcid.org/0009-0000-9076-6410

[1] Independent Researcher, Uruana de Minas, Minas Gerais, Brazil

* Correspondence: Lucas Giovani Ribeiro, coin26@mail.com

Co-author email: thecygnuscode@gmail.com

Abstract

Preserved architectural geometry can constrain the missing form of a damaged object. We derive a reversible relation linking the sarcophagus, King's Chamber and exterior profile of Khufu's Great Pyramid. In a centred chamber section, equating a crossed-line rise to each lateral gap reconstructs length and profile angle from three preserved interior dimensions, without a fitted continuous coefficient. Petrie's measurements yield a 2.303-m envelope and a 51.838° profile, differing from his historical comparisons by 1.69 mm and 23.7 arcsec. The relation alone matches length within 0.2% among 127 declared rule classes and retains the best central length fit in expanded rule families. An additional volume constraint also recovers sarcophagus height. Architectural context thus supplies a quantitative constraint on lost form, with explicit predictions for independent surveys of the damaged ends and original position.

Introduction

Khufu's Great Pyramid at Giza, Egypt, was built about 4,500 years ago as a royal funerary monument [1]. Its granite King's Chamber contains a stone sarcophagus, also called the coffer, whose damaged ends and disturbed position complicate reconstruction of its original form and arrangement [2]. The surviving chamber provides a further source of information about the damaged object: the spatial relationships linking its envelope to the surrounding architecture. We test a reversible relation that uses preserved interior dimensions to recover the missing sarcophagus length and generate a profile compatible with the pyramid's exterior inclination. This turns the architectural setting into a quantitative reconstruction constraint and makes original placement part of the same testable geometric problem.

Recent investigations have made the Great Pyramid an active setting for non-invasive heritage science. Muon imaging identified the Big Void and characterized the North Face Corridor [1,3], while combined radar, ultrasound and electrical-resistivity imaging examined the corridor through complementary physical measurements [4]. Ultrasonic investigation of the King's Chamber masonry [5] and characterization of stone surfaces in the inner chambers [6] address surviving construction and material condition. These studies establish the contemporary documentation context. They do not independently measure the missing sarcophagus ends or recover its original position, which are the distinct validation targets of the present reconstruction.

Computational studies also make architectural hypotheses explicit and testable. Rosell Roig [7] evaluates a proposed construction system for the Great Pyramid through a computational model. Here, the object of inference is the damaged sarcophagus envelope and its geometric relation to the chamber and exterior

profile. The practical issue is how to distinguish a reproducible relation in historical measurements from an arrangement supported by independent material evidence.

Studies of architectural reconstruction offer complementary ways to constrain missing form. Meriggi et al. [8] combine non-invasive observations and structural equilibrium to assess partially preserved Roman architecture. Apollonio et al. [9] distinguish uncertainty in geometry, construction, surface appearance and position in hypothetical models. Vaienti et al. [10] use historical drawings and parametric modelling to reconstruct Leonardo da Vinci's centrally planned churches. We use metrological closure: a relation among preserved measurements generates quantities that can be compared with a damaged component and an independently surveyed exterior. Historical documentation, assumed placement and derived geometry retain separate evidential roles.

Petrie's detailed chamber and sarcophagus measurements, supplemented by later exterior and orientation surveys, provide the historical basis [2,11,12]. Chamber width and height and sarcophagus height are preserved dimensions; original sarcophagus length is inferred from damaged end surfaces; pyramid inclination is surveyed outside the chamber. A useful coupling must keep these roles explicit. It must also be compared with alternative rules, because a monument containing many dimensions permits numerous approximate correspondences.

The starting observation was geometric: lines joining the upper chamber corners to the opposite upper sarcophagus corners appear to produce two opposed pyramid profiles sharing an apex. The larger profile spans the chamber; the smaller spans the reconstructed sarcophagus length. Photographs motivated the construction but cannot validate it because perspective, distortion, damage and displacement affect their appearance. Figure 1A–B shows the sarcophagus and its setting. The quantitative test uses a centred orthographic section and documented dimensions (Figure 1C–E).

The decisive step is closure from inside the chamber. Exterior inclination can invert the crossed-corner equation to recover sarcophagus length, but then enters as an input. In the internal construction, the lower X rise D equals each lateral gap g. Given only chamber width W, chamber height H and sarcophagus height h, this equality returns original length L and profile angle θ. Under D=g, the ideal $\tan\theta=14/11$ is equivalent to $L/W=11/25$ and $(H-h)/W=252/275$. Introducing the independently measured exterior base as a subsequent scale check gives opposed profiles approximately 1:44 and 1:100 of the exterior pyramid.

The relation was identified retrospectively with knowledge of the historical record. Its evaluation separates computational inputs from comparison quantities and tests the construction through a declared rule grammar, physical-role and position tests, sensitivity analyses and comparative controls. Frozen specifications preserve reproducibility; blinded morphology and placement protocols provide the next tests against independent material evidence.

The study asks whether D=g reconstructs the damaged envelope and exterior profile without exterior inputs, whether it is specific within a declared family of comparable rules, and whether its success depends on the selected physical dimensions and placement. It also tests the relationship to Petrie's published proportions and explores whether his historical volume-balance criterion can extend the reconstruction to sarcophagus height.

The contribution is a reconstruction framework in which missing object dimensions remain constrained by surviving relationships with their architectural setting. For Khufu, one internal equality connects the sarcophagus envelope, chamber proportions and exterior profile, while predicting distinct effects of end damage, sideways displacement and altered vertical clearance. These effects separate the evidence needed

for form, position and profile and define measurements for an independent documentation campaign. Supporting derivations and numerical tables appear in Supplementary Information, Part I; the executable archive is supplied as Supplementary Data 1.

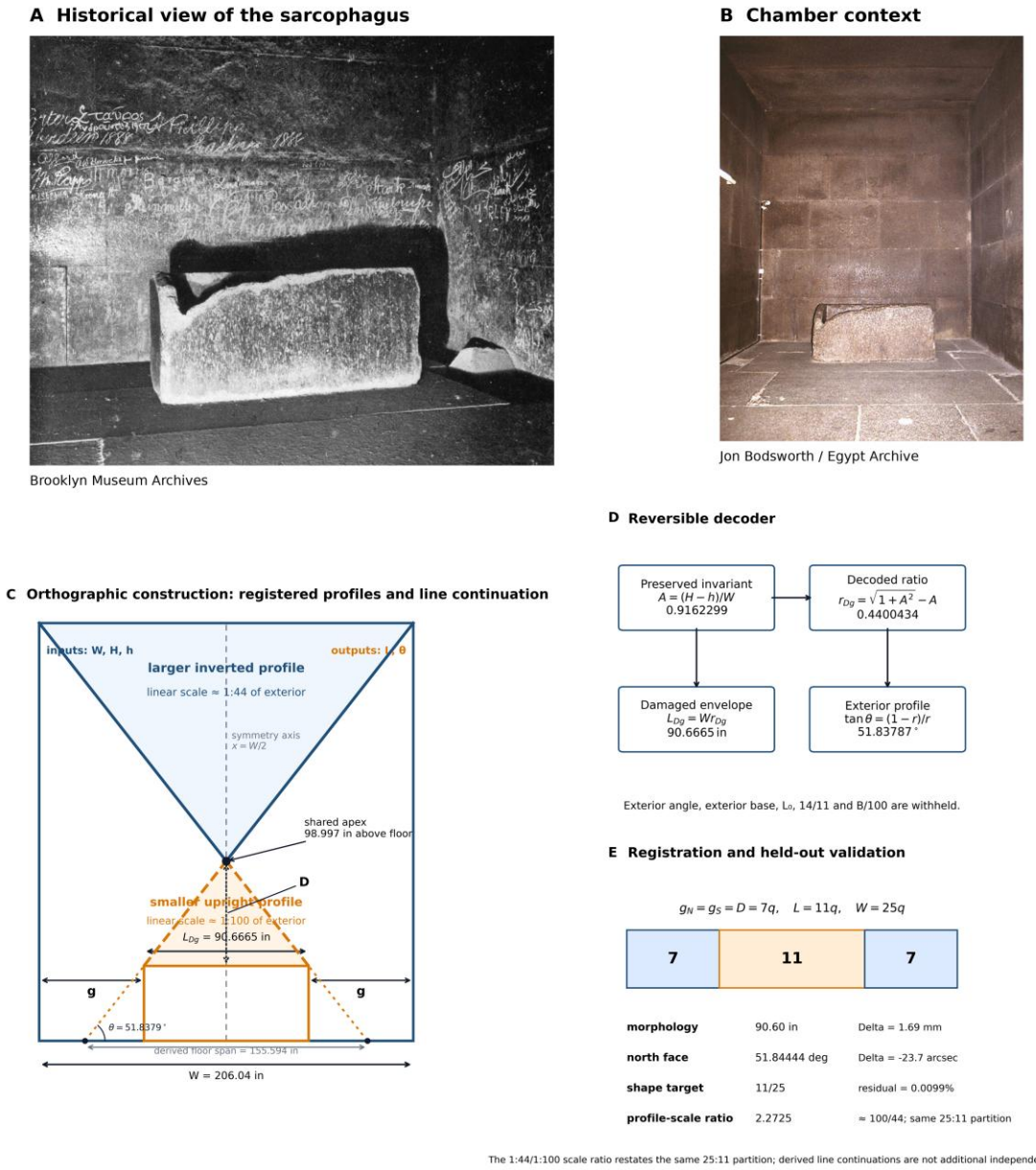


Figure 1. Sarcophagus context and reversible internal relation. (A) Archival view showing the damaged upper edge and surrounding masonry. Brooklyn Museum Archives, Lantern Slide Collection, S10|08 Gizeh, image 9620; attributed to William Henry Goodyear, Joseph Hawkes and John McKecknie; no known copyright restrictions. (B) Chamber view by Jon Bodsworth / Egypt Archive, authorised for unrestricted reuse. Both photographs are reproduced via Wikimedia Commons without cropping or retouching; source files and rights records accompany Supplementary Data 1. They provide documentary context, not survey measurements or evidence of original placement. (C–E) Preserved W,H,h generate L and θ through D=g; the decoder and registration checks express the same relation. Opposed profiles at approximately 1:100 and 1:44 share an apex 98.997 in above the floor. Dotted continuations and nested subdivisions add no independent constraints. Source for C–E: authors' calculations. Angles refer to the orthographic projection normal to the west wall.

Methods

Petrie's chamber and sarcophagus survey

Petrie treated the King's Chamber as one of the best-measured parts of the pyramid. He documented wall separations, course heights, levels, opened joints and structural movement, and distinguished corrected architectural quantities from the room's disturbed present state [2] (pp. 79–83). The crossed-corner construction begins at the upper corners of the west end wall. The point-specific corrected width is W=206.04 in; the chamber-wide mean of 206.12 in is retained as a sensitivity alternative.

The granite sarcophagus was reduced from hundreds of surface offsets and independent calliper measurements to mean planes. Petrie reported a current mean external length of 89.62 in, external width 38.50 in and external height h=41.31 in, together with internal length 78.06 in, width 26.81 in and depth 34.42 in [2] (pp. 84–90). Both ends are damaged. From surviving curvature and straight-edge comparison, he reconstructed a maximum original external length near L0=90.60 in and separately noted its proximity to one hundredth of the pyramid base [2] (pp. 197–199). The 90.60-in value is therefore morphology, not an intact measurement, and no modern probability interval accompanies it.

Petrie also evaluated the coffer volumetrically. Using mean planes he reported contents of 72,030 in³, solid bulk of 70,500 in³ and total rectilinear volume of 142,530 in³; he later described the near equality of contents and solid bulk as an inexact relation that might at most reflect a rough design intention [2] (§§61, 156). The present study uses volume balance as a secondary historical check and, in a retrospective extension, combines it with D=g to reconstruct both coffer length and height. The primary D=g decoder remains unchanged.

Petrie's measured wall clearances describe the present position, not the original installation. The four paired corrections required to equalise the north and south gaps average 9.64875 in southward. The object was also lifted, tilted and damaged, and Petrie reported no surviving placement lines. The original transverse offset is therefore an unrecovered quantity with a separate frozen protocol.

Exterior profile and reduced proportional baseline

The Great Pyramid's face is commonly expressed by the Egyptian seked. A seked of 5 1/2 palms corresponds to a horizontal run of 11 for a vertical rise of 14, or modern rise/run 14/11 and an angle near 51.8428 degrees [13,14]. Petrie's weighted north-face value is 51 degrees 50 minutes 40 seconds with a reported uncertainty of approximately 1 minute 5 seconds. The measured face, rather than the nominal ratio, is the primary exterior comparison.

The conventional seked describes the exterior proportion. The question here is whether preserved interior measurements independently reconstruct that profile through a reversible coupling.

Petrie also published two internal proportional observations: H/W is close to sqrt(5)/2 and h/W is close to 1/5 [2] (§§155–156). These proportions explain much of the broad angular neighbourhood and must be retained as a reduced alternative. They do not, by themselves, specify the crossed endpoints, the equality D=g, the required centring or the recovery of the broken envelope. The historical record therefore permits a strong structural comparison but only partial discrimination between the full measured construction and the complete reduced proportional family.

From reverse engineering to a falsifiable construction

Reverse engineering supplies the hypothesis; low complexity, reversibility, physical roles, withheld outputs and tests capable of failure carry its evaluation. The proposed instruction is the unit equality D=g between two defined orthographic segments.

Dimensional encoding is an operational description of the reversible relation among quantities omitted from the solver inputs. Specificity, physical realisability and positional registration can constrain a proposed construction, but the original placement must be independently established before inferring historical implementation. Symbolic meaning and the builders' conceptual language require additional historical evidence.

Frozen variables and evidential classes

Table 1 gives the primary quantities and SI equivalents alongside Petrie's original inch values (1 in = 0.0254 m exactly). Calculations retain the source units to avoid conversion rounding; all main relations are unit-invariant, and converted digits do not imply additional measurement precision. Preserved measurements are W, H and h. Reconstructed morphology is L0. Exterior observables are B and the north-face inclination. The present offset is an ablation value; the original offset remains unknown. This classification prevents a reconstructed or exterior quantity from entering the internal decoder unnoticed.

Notation. W, transverse chamber width; H, free chamber height; h, external coffer height; L, external envelope length; L0, morphology-based length; G=H−h, upper vertical difference; U,D, upper and lower intersection rises; g, one-sided gap; A=G/W; r=L/W; θ, profile angle; B,Z, exterior base and height; W_e, external coffer width; l_i,w_i,d_i, cavity length, width and depth; K=2l_iw_id_i/W_e; δ, transverse centre offset; τ, tolerance; z, physical coffer-base elevation. Subscripts identify source, state or decoder; asterisk identifies joint reconstruction.

Table 1. Measurement provenance and evidential role

Quantity	Symbol	Value	Measurement class	Role
West-wall top width	W	206.04 in (5.233416 m)	corrected architectural length	internal decoder input
Mean chamber width	Wmean	206.12 in (5.235448 m)	mean architectural length	role sensitivity
Free chamber height	H	230.09 in (5.844286 m)	level-network derivation	internal decoder input
External sarcophagus height	h	41.31 in (1.049274 m)	preserved mean plane	internal decoder input
Current external length	Lcurrent	89.62 in (2.276348 m)	damaged mean plane	state control
Original external length	L0	≈90.60 in (≈2.301240 m)	morphological reconstruction	withheld validation
Mean exterior base	B	9068.8 in (230.34752 m)	exterior survey	downstream scale check
North-face inclination	thetaN	51°50′40″ ±1′05″	exterior survey	downstream angle check
Present transverse correction	delta current	9.64875 in (0.245078250 m)	wall-clearance pairs	position ablation

Quantity	Symbol	Value	Measurement class	Role
Original transverse offset	delta0	unrecovered	independent historical state	prospective endpoint
External sarcophagus width	W_e	38.50 in (0.977900 m)	preserved mean plane	supplementary R12/R13 input
Internal cavity length	l_i	78.06 in (1.982724 m)	preserved mean plane	supplementary R12/R13 input
Internal cavity width	w_i	26.81 in (0.680974 m)	preserved mean plane	supplementary R12/R13 input
Internal cavity depth	d_i	34.42 in (0.874268 m)	preserved mean plane	supplementary R12/R13 input

Orthographic X and intersection geometry

Here L denotes the longitudinal extent of the ideal rectangular body envelope in the orthographic projection normal to the west wall. Its morphological comparator must distinguish that extent from surviving mean-plane length and from spans altered by end-face skew or rotation. The reported θ is an angle in this projection, not the inclination of a spatial line joining points separated in depth.

Represent the transverse chamber section by a rectangle of width W and free height H. Represent the original sarcophagus envelope by a rectangle of length L and height h, centred laterally. The upper chamber corners are (0,H) and (W,H); the upper sarcophagus corners are ((W-L)/2,h) and ((W+L)/2,h). Each crossed branch has vertical rise H-h and horizontal run (W+L)/2, so

$$tan(\theta_X) = \frac{2(H-h)}{W+L} \quad (1)$$

Internal decoder D=g

Let G=H-h. The two branches intersect at x=W/2. Similar triangles divide G into an upper height U=GW/(W+L) and lower height D=GL/(W+L). The one-sided lateral gap is g=(W-L)/2. The proposed primitive instruction is

$$D = g \quad (2)$$

Equating the two segments and solving the positive physical root gives

$$L_{Dg} = \sqrt{(H-h)^2 + W^2} - (H-h) \quad (3)$$

The same relation is clearer in dimensionless form. Define A=(H-h)/W and r_Dg=L_Dg/W. Then

$$A = \frac{1 - r_{Dg}{}^2}{2r_{Dg}} \quad (4)$$

and inversion gives

$$r_{Dg} = \sqrt{1 + A^2} - A \quad (5)$$

Once r_Dg is known, the envelope length follows without an exterior input:

$$L_{Dg} = W r_{Dg} \quad (6)$$

The construction is fully reversible. Any one of A, r_Dg or the profile tangent determines the other two. The direct crossed-corner angle calculated from a supplied L remains tan(theta_X)=2(H-h)/(W+L); under D=g it reduces identically to (1-r_Dg)/r_Dg.

$$tan(\theta_{Dg}) = \frac{1 - r_{Dg}}{r_{Dg}} \quad (7)$$

The same equality has a direct diagonal construction. Completing the square in $L^2+2GL-W^2=0$ gives

$$(G + L)^2 = G^2 + W^2, \quad L = C - G, \quad C = \sqrt{G^2 + W^2} \quad (7a)$$

Thus L is the diagonal of the W-by-G rectangle minus its height G (Figure 2A). This is an exact geometric restatement of D=g. Equation (7) also makes the seked connection explicit: under D=g, tan θ=14/11 is equivalent to r=11/25 and A=252/275. The equality D=g relates the variables; the measured A determines the resulting slope.

Registration layers: form, position and scale

The shape code is the reversible A-to-r_Dg mapping. A centred physical placement adds positional registration: g_N=g_S. The equality D=g then repeats the same module twice horizontally and once vertically, g_N=g_S=D. For the ideal target r_Dg=11/25, the width decomposes as 25=7+11+7. This is redundant registration of one relation, not three independent coincidences.

The historical vertical registration h/W≈1/5 is unnecessary for decoding L or θ. The downstream exterior check B/W≈44 is compatible with shared cubit metrology. Its conjugate fit with L≈B/100 and D≈Z/100 follows from B/44=B/100+2Z/100 under the 440:280 profile. These relations are dependent checks, not independent probabilities.

Downstream validation and exterior-input checks

The internal decoder withholds the damaged length, exterior angle, exterior base, 14/11 and B/100. Its primary validations are the morphological L0 and measured north-face inclination. This study reports central differences, not Gaussian significance, because the historical bounds combine survey corrections, surface variation and reconstruction uncertainty.

As a complementary downstream validation, the exterior angle can also be used in the opposite direction:

$$L_\theta = \frac{2(H - h)}{tan(\theta_{face})} - W \quad (8)$$

Petrie's historically specified centesimal comparison gives L_B=B/100. These are distinct exterior-based checks based on different measured observables, but they are not treated as statistically independent evidence within the integrated code network. The reduced H/W, h/W angular branch and the reduced centesimal branch are retained to quantify partial discrimination.

Five-panel specificity audit

R10.1 enumerates equalities between 13 physical segments using the operators, exclusions and root-equivalence criterion in Table 2. Length and tangent residuals are reported separately; closure requires both below tolerance. Classes are descriptively ordered by their maximum residual. Integer partition and scale ratios are unscored. At fixed W,H,h, tangent depends deterministically on L; R13 measures criterion contributions without changing the frozen comparison. Archive module labels are retained for reproducibility.

Table 2. Declared rule grammar and selection criteria

Component	Frozen specification
Segment vocabulary	L, L/2, W, W/2, H, h, G, G/2, g, D, U, W−L, Y=h+D; G, g, D and U are defined in th Orthographic X and Internal decoder subsections.
Operators	x=y; x=2y; 2x=y; x=y+z; x=y−z.
Admissible roots	30<L<W−30 in; exclude tautologies and L-independent residuals.
Equivalent classes	Group roots by L rounded to 10^{-4} in; retain equivalent expression counts.
Comparison criteria	e_L=|L_pred−90.60|/90.60; e_θ=|tan θ_pred/tan θ_N−1|. Report separately; closure r both ≤0.2% (additional bands: 0.5%, 1%, 2%).
Enumeration	1,950 expressions; 16 tautologies and 229 L-independent expressions; 476 admissibl instances; 127 classes.
Unscored outputs	7|11|7 partition, B/W≈44 and B/L≈100. Maximum residual ranks classes descriptivel adds no rejection to length selection.

Panel 1 enumerates rules. Panel 2 draws 400,000 geometries (seed 21): W uniform on 150–280 in, H/W on 0.9–1.4 and h/W on 0.15–0.30. It separates the specific 11/25 target from reduced rationals with denominator ≤30; R11 analytically integrates the same target interval. Panel 3 tests 32 role assignments. Panel 4 varies offset under max(|g_N−D|,|g_S−D|)≤τg. Panel 5 transfers the operator to the Queen's Chamber and compares Hawara; R16 subsequently extends the Hawara body-section comparison to the whole grammar. These are conditional audits, not universal chance probabilities.

For reproducibility, pairwise expressions are generated from unordered segment pairs and three-term expressions from distinct triples with the implementation's fixed lexical ordering for the final two terms. R10.1 excludes identities and residuals independent of L, retains exact-grid and sign-changing roots on a 2,001-point grid, and refines the latter with 80 bisection steps. Admissible roots are stored to six decimals and grouped by rounding L to four decimal places. R16 independently clears the positive denominator W+L and solves polynomials of degree at most two, checking the roots in the original segment functions. The lexical expression convention and rounded classes define the stated grammar; no completeness over other grammars is assumed.

The specific rational-target error is |r/(11/25)−1|. For the generic comparison, the minimum |r−p/q|/r is taken over reduced fractions with denominator q≤30. Exact integration uses X=H/W uniform on [0.9,1.4] and Y=h/W uniform on [0.15,0.30]. The density of A=X−Y is max(0,min(0.30,1.4−A)−max(0.15,0.9−A))/0.075. Its piecewise-linear integral is evaluated between the images of r=(11/25)(1±τ) under A=(1−r²)/(2r). The 32 role assignments use four W candidates (206.04, 206.12, 412.24 and 38.50 in), two H candidates (230.09 and 235.20 in) and four h candidates (41.31, 34.42, 6.89 and 5.11 in), with their source-defined physical roles retained.

Supplementary historical coffer-volume check

R12 tests Petrie's inexact historical contents–bulk relation using rectilinear mean planes: V_c=l_iw_id_i, V_env=LW_eh and V_g=V_env−V_c. Ideal V_c=V_g gives L_V=2V_c/(W_eh). Cavity dimensions and W_e=38.50 in do not enter the primary decoder. The retrospective balance is an idealised, non-scored cross-check; its bounded-domain frequency is sensitivity only and is not combined probabilistically with R10.1/R11.

Joint reconstruction of coffer length and height

R13 combines the two previously analysed relations while treating external length and height as unknowns. Set K=2l_iw_id_i/W_e, so the ideal volume balance becomes Lh=K. Substituting h=K/L into the D=g quadratic gives $L^2+2HL-W^2-2K=0$ and its unique positive root:

$$L_* = \sqrt{H^2 + W^2 + 2K} - H \quad (9)$$

$$h_* = \frac{K}{L_*} \quad (10)$$

Inputs are W,H,W_e,l_i,w_i,d_i; h, L0 and exterior inclination are comparison quantities. R13 verifies the root by bisection and substitution. This retrospective, non-scored extension inherits ideal volume balance and shared survey data. Sensitivities vary the existing R01 W,H bounds with cavity dimensions and coffer width fixed (Supplementary Information, Part I, S21).

R14 substitutes h=K/L into all 1,950 expressions, retaining the original vocabulary and admissible interval. Every rule receives the same volume condition. Admissible roots are grouped as in R10.1 and ordered by length residual; length and height use the existing 0.2% tolerance. This exploratory extension leaves the frozen panel unchanged (Supplementary Information, Part I, S22; archive in Supplementary Data 1).

For the joint grammar, multiplication by the positive denominator 2L(W+L) yields polynomials of degree at most three. Exact rational coefficients are used before numerical root finding; real roots in the original admissible interval are retained and grouped by the same rounding convention. A separate direct-function implementation brackets roots and refines them with Brent's method. The original fixed-height classes are reproduced before evaluating the extension. This verification concerns numerical implementation, not the accuracy of historical measurements.

State, position and comparative controls

The current damaged length is substituted as a state control, the crossed-corner geometry is rotated as a descriptive axis check, and ten same-survey dimensions are substituted for L. Petrie's present transverse offset is applied directly to the two arms. The Queen's Chamber supplies two distinct controls: its finished gable is a built-triangle control, while transferring the D=g operator tests whether a similar-width chamber automatically supports the same decoder. No sarcophagus survives there, so it is not a homologous chamber-coffer control.

Hawara uses the documented transverse section with equal lateral clearances: chamber W=94.2 in, H=92.4 in, coffer h=55.5 in and measured width 48.4 in [15] (§§17, 25–26). R16 transfers the complete grammar to this body section using both the original 30-in exclusion and the proportional domain $30/206.04<L/W<1-30/206.04$. The three reported exterior fragments are alternative references for one monument. Sources, eligibility criteria and implementation checks are documented in Supplementary Information, Part I, S24.

The Queen's Chamber transfers use W=205.85 in and either wall-top H=184.47 in or gable-apex H=245.10 in, retaining h=41.31 in only as an operator-transfer input. Hawara's exterior references are 48.75°, 49.85° and 52.416667° from three fragments of the same monument. Eligibility requires documented physical endpoints, a comparable body section and adequate dimensional provenance; non-homologous or unresolved cases are not scored as negative results. For the optional root-density diagnostic, the union of target intervals [L_pred/1.002,L_pred/0.998] is clipped to the declared admissible

domain and divided by its length. This diagnostic is a conditional coverage measure, not an empirical false-positive rate.

Bounds and prospective protocols

Historical ranges are bounded sensitivities, not standard deviations. Protocol A retains its frozen core of 90.404–90.789 in and broad envelope of 89.750–91.412 in. Frozen before D=g for measured-face inversion, these bands test compatibility and reduced alternatives rather than specifically confirming D=g. The decoder's point prediction is recorded without changing them. Protocol B seeks original-position traces or archival coordinates. Neither uses a new scan; R10.1 does not replace their decision bands (Supplementary Information, Parts II and III).

The historical sensitivity box is $W\in[205.92,206.16]$, $H\in[229.94,230.24]$ and $h\in[41.14,41.50]$ in. Corner evaluations preserve these bounds without assigning probability distributions. In a level section with $a=(W+L)/2$ and transverse offset δ, the two tangents are $G/(a+\delta)$ and $G/(a-\delta)$; their reciprocal sum recovers the centred tangent algebraically. A physical base elevation z changes G to $H-h-z$, whereas translating the coordinate origin does not change G. Local derivatives and exact substitutions quantify these effects without fitting a datum shift.

For the lid sensitivity, the documented ledge depth is 1.70 in and the effective level endpoint height is $h_{eff}=h-1.70+t$, where t is the thickness above the seating surface. The existing 0.2% length band is inverted through the same decoder to obtain the allowable endpoint-height interval. The hypothetical lid calculations do not infer a surviving or original lid thickness. The historical volume-domain sensitivity integrates the allowable external-width interval analytically and uses 64-point Gauss–Legendre quadrature over the remaining declared dimensions; its domain definitions and outputs are retained in R12 and are not combined with the primary rule comparison.

Exploratory reconstruction audit

R15 compares seven reconstruction routes with their inputs and assumptions explicitly distinguished, evaluates all eight corners of the existing W,H,h bounds, and substitutes Smyth's historical measurements (Supplementary Information, Part I, S23). Exterior-angle inversion uses the angle as an input; its angular closure is not validation. R16 verifies the transferred polynomial implementation against all 127 stored Khufu class lengths and evaluates the lid surface as a distinct reference state (Supplementary Information, Part I, S24). Both audits are retrospective; the bounds are sensitivity ranges, not confidence intervals.

R17 tests robustness by extending the same 13-segment grammar to all primitive integer-coefficient relations involving two or three distinct segments. The admissible length interval and root grouping are retained. The sum of absolute coefficient values defines budgets of three, four and five. A grid of 21 equally spaced values within each existing W,H,h bound supplies 9,261 scenarios. Supplementary Information, Part I, S25 reports central ranking, input sensitivity and threshold acceptance; the original R10.1 specification and prospective protocols retain their frozen definitions.

The two prospective protocols have not been executed. For the envelope test, calibrated scans must cover both damaged ends and the preserved long faces; analysts fit the longitudinal axis and reconstruct missing surfaces without the geometric targets. The frozen specification retains polynomial, regularised-spline and uncertainty-bearing smooth-surface families, a median point estimate and the union of their 95% intervals, with registration and held-out reconstruction checks. For position, eligible traces or archival coordinates must predate disturbance and support an uncertainty interval. Both analyses lock exclusions,

code and reports before unblinding. The full unchanged decision rules are reproduced in Supplementary Information, Parts II and III.

Results

Preserved internal dimensions recover the damaged envelope and exterior profile

Equations (5)–(6) give A≈0.91623, r_Dg≈0.44004 and L_Dg=90.67 in. The central difference from Petrie's approximately 90.60-in morphology is 1.69 mm. Using the chamber-mean width increases L by 1.50 mm; varying H by ±0.15 in changes L by approximately ∓1.24 mm. The agreement is therefore of the same order as input sensitivity. Petrie's reconstructed target has no calibrated uncertainty distribution.

Equation (7) gives θ=51.838°, 23.7 arcsec below Petrie's north-face value of 51°50′40″ and within his ±65-arcsec band. Neither exterior quantity was used to obtain L or θ.

Using Petrie's morphological L0≈90.60 in directly in the crossed section gives an angle 1.19 arcsec below his north-face value. The internally recovered length and morphology-based envelope therefore return closely agreeing exterior profiles.

One relation connects form, position and scale

The internally derived ratio is r_Dg=L_Dg/W=0.4400434, differing from 11/25 by 0.00986%. In the corresponding 25-part representation, L=11.0011 parts and each lateral gap is 6.9995 parts. Because D=g exactly under the decoder, the same seven-part module is registered twice horizontally and once vertically. The geometric content is therefore the redundant pattern 7|11|7 with D=7, not seven independent numerical matches.

The known vertical ratio h/W=0.200495 differs from 1/5 by 0.2475%. Introducing B only downstream gives B/W=44.0148 and B/L_Dg=100.0237. Two opposed similar profiles share an apex 98.997 in above the floor: the upright coffer profile at approximately 1:100 and inverted chamber profile at approximately 1:44. Their scale ratio differs from 100/44 by 0.0099%, restating the transverse 25:11 partition rather than adding evidence.

Continuing the same lines gives floor intercepts x=25.223 and 180.817 in and span 155.594 in. The floor triangle and flanking subdivisions retain θ=51.8379°. Around x=W/2, eight drawable right-triangle manifestations, some nested, illustrate one line direction without new fitted slopes or independent constraints.

The recovered face-normal profile is common to all faces of an ideal symmetric square pyramid. The interior construction remains axis-specific: replacing W by chamber length 412.24 in, with other quantities fixed, gives 36.8976° and a 41.0% slope departure. This descriptive rotation is unscored. Outputs and downstream checks appear in Table 3.

Table 3. Internal decoder outputs and downstream checks

Quantity	Expression	Value	Interpretation
Internal invariant	A=(H-h)/W	0.916229858	preserved W,H,h only
Decoded ratio	r_Dg=sqrt(1+A²)-A	0.440043401	0.00986% from 11/25

Quantity	Expression	Value	Interpretation
Decoded original length	L_Dg=Wr	2.302930 m (90.666542 in)	1.69 mm from morphology
Decoded profile	atan((1-r)/r)	51.837871°	−23.67 arcsec from north face
Measured-face inverse	2(H-h)/tan(thetaN)-W	2.301151 m (90.596477 in)	exterior-based check
Centesimal check	B/100	2.303475 m (90.688 in)	historically specified check
Scale checks	B/W; B/L_Dg	44.0148; 100.0237	downstream, algebraically connected
Historical volume-balance inverse	2l_iw_id_i/(W_eh)	2.300827 m (90.583750 in)	0.41 mm from morphology; 2.10 mm from L_Dg; non-scored R12

A historical coffer-volume balance separately reconstructs the damaged envelope

Petrie's mean-plane inputs reproduce his reported contents and granite volumes to within 3.8 and 1.0 in^3, respectively. Imposing ideal contents–bulk balance gives L_V=90.58 in: 0.41 mm below morphology and 2.10 mm below D=g. Restoring the envelope nearly closes the volume discrepancy, but this idealised retrospective check remains non-scored (Supplementary Information, Part I, S9A).

Joint reconstruction recovers the external coffer height

Solving D=g and the ideal volume balance together yields L*=90.66 in and h*=41.28 in, differing from the morphology-based length and measured height by +1.42 and −0.83 mm. Height becomes an output rather than an input (Figure 2B). The slope is 51.844°, 2.62 arcsec below the north-face central value.

The joint angle remains input-sensitive: the existing H bounds give residuals from −86.3 to +81.0 arcsec. This reconstruction combines two existing relations; it supplies no new observation or independent replication (Supplementary Information, Part I, S21, Table S12).

Under the same volume condition for every rule, the 1,950 expressions yield 559 admissible roots and 154 classes. Only D=g recovers length within 0.2%; its length and height errors are 0.0617% and 0.0796%. The nearest length competitor, H=2(W−L), gives 0.436% and 0.452%. The selected relation thus persists when height is reconstructed. Height adds no rejection because Lh=K links the outputs (Supplementary Information, Part I, S22, Table S13).

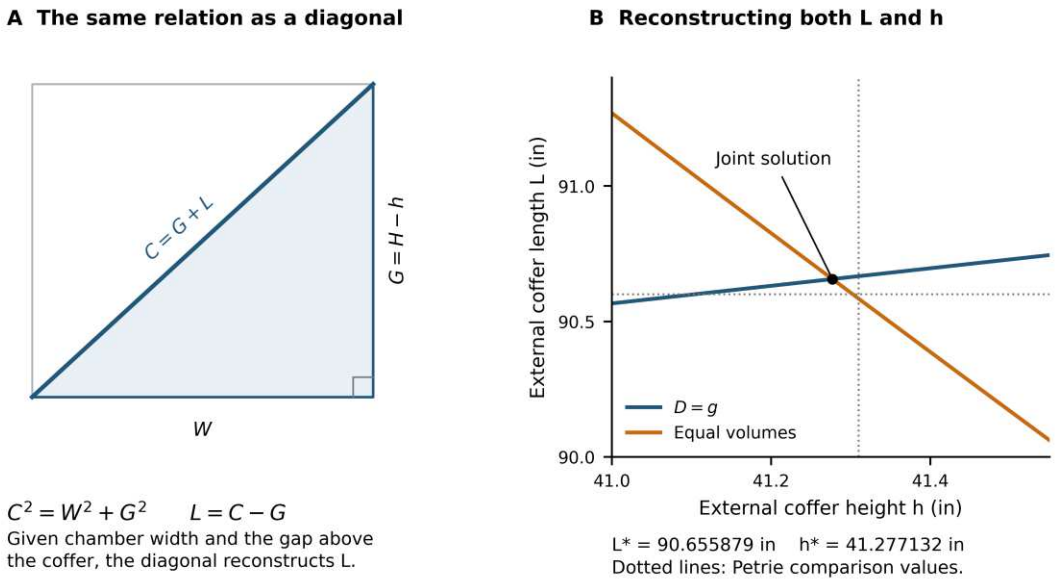


Figure 2. Diagonal and joint reconstruction. (A) L is the W-by-G diagonal minus G. (B) Geometric and ideal volume-balance curves intersect at L*,h*. Dotted comparisons are Petrie's values; sensitivity is in Table S12. The panels restate existing relations. Source: authors' calculations.

The declared rule comparison selects one closing class

The grammar generates 1,950 expressions; after exclusions, 476 physical roots collapse to 127 classes. Only D=g recovers the withheld length within 0.2%, with length and tangent errors of 0.0734% and 0.0236%, represented by 13 equivalent expressions. Three classes satisfy the tangent criterion; one satisfies both. The angular filter therefore adds no rejection to length selection. Tangent residuals are 0.24–0.38 times length residuals across the panel: the measured face is a distinct survey comparison, but the acceptance criteria are dependent. The runner-up H=2(W−L) gives L=91.00 in and a 0.436% length error; its worst-channel residual is 5.936 times larger.

At 0.2% tolerance, 47.29% of Monte Carlo geometries lie near some reduced rational with denominator ≤30: an unspecified simple rational is common. The specific 11/25 target occupies 1.0828%; exact integration gives 1.0851%, verifying the simulation. These frequencies apply to the declared uniform domains, not a universal chance model.

Two of 32 physical-role assignments closed at 0.5%; they use the west-wall top width and chamber mean width, respectively, and therefore belong to the same physical width class. The third-ranked assignment already has a 3.2025% tangent residual. Rule uniqueness, target frequency and role dependence are distinct results: the first concerns the grammar, the second the declared geometry null, and the third the assignment of measured quantities. The specificity audit is summarised in Figure 3.

D=g retains the best central length fit as the comparison expands from 127 to 338 and 686 rule classes. Completing all term orientations at coefficient budget three reproduces the original 127 classes. At budget four, D=g remains the sole central match within 0.2%; at budget five, 3L=H+h also meets both thresholds, with a 0.1472% length error. The joint volume-constrained extensions likewise retain D=g as the best central length fit within each enlarged rule family (Supplementary Information, Part I, S25, Tables S15–S16).

Across all 9,261 bounded-input scenarios, D=g remains the closest length prediction within the original grammar, with a minimum advantage of 1.890 mm over the nearest competitor. It meets the length threshold at 8,712 points; every alternative original rule stays outside that threshold throughout the grid. At coefficient budget five, D=g ranks first in 4,998 scenarios (54.0%), while at least one alternative meets the 0.2% length criterion in 9,222 (99.6%). Figure 3D–F maps the minimum error advantage over all 21 heights at each width–height pair; the expanded families show lower ranking stability (Table S17). These are counts across deterministic scenarios, not probabilities.

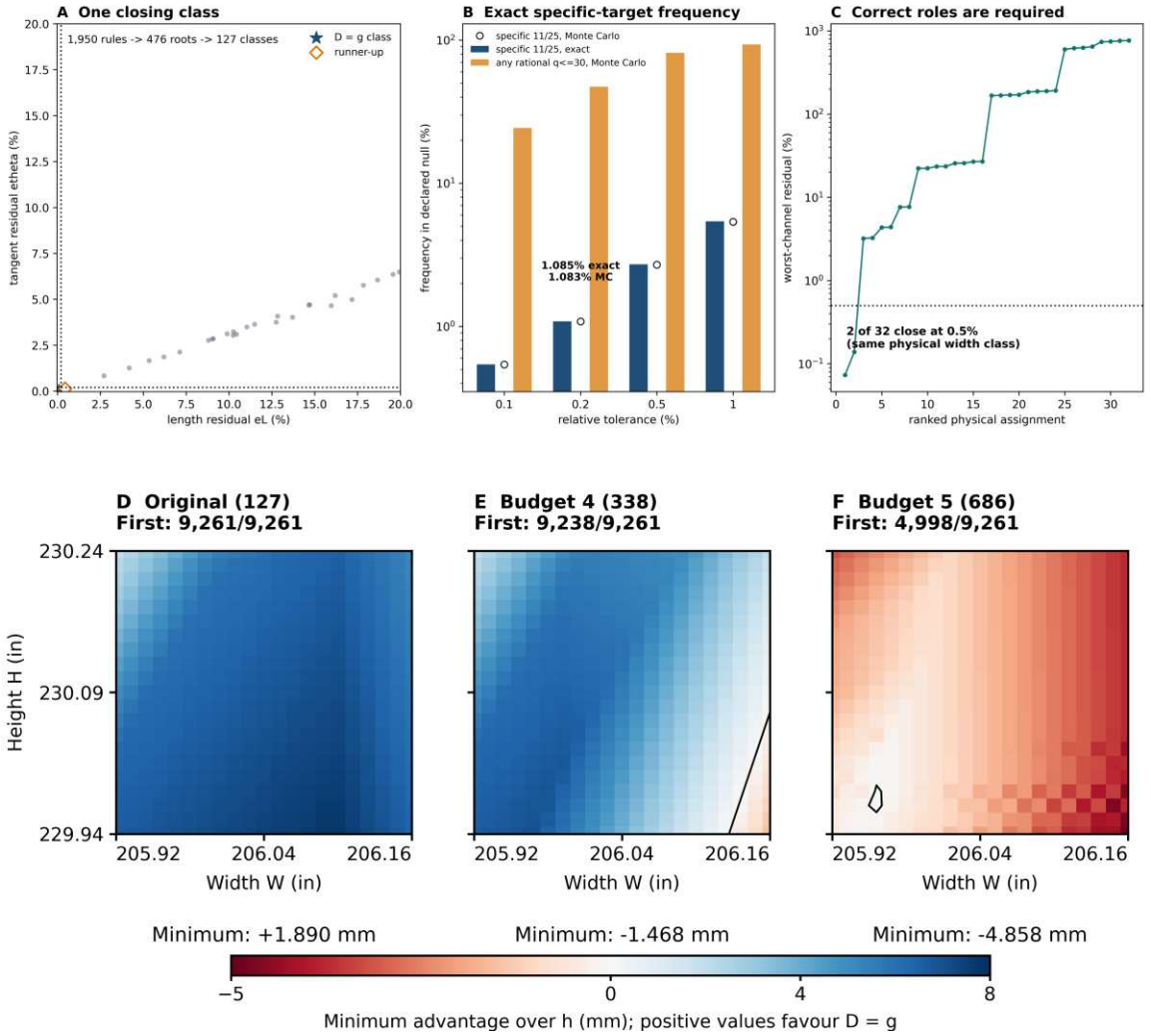


Figure 3. Specificity and bounded-input robustness. (A) Within the original grammar, D=g alone matches length within 0.2% among 127 classes; tangent adds no rejection. (B) Exact and simulated specific-target frequencies agree; unspecified simple rationals are common. (C) Two closing role assignments share one width class. (D–F) R17 length-error advantage over the nearest alternative in the original grammar and expanded budgets four and five. Advantage equals the alternative's absolute length error minus D=g's, relative to L0=90.60 in. Each map cell shows the minimum over all 21 coffer heights h=41.14–41.50 in at the indicated W,H; positive values favour D=g at every tested h, and the black contour marks zero. Counts above the panels refer to the full 21×21×21 grid, not the projected map. Source: authors' calculations from the archived R17 results (Table S17).

Exterior-based checks remain consistent but discriminate only partially

Measured-face inversion gives L_θ=90.60 in; B/100 gives 90.69 in. Both, the internal decoder and the morphological target lie in the frozen core. The reduced centesimal branch 0.44W=90.66 in also lies inside it.

The reduced H/W=√5/2, h/W=1/5 composition instead gives 91.18 in under measured-face inversion, outside the core but inside the broad envelope. Its separation from the measured-input inversion is 14.84 mm. The frozen band discriminates against this angular branch, but does not exclude the reduced family because its centesimal branch remains in the core. Like-for-like angle conventions and full-precision values are retained in Supplementary Information, Part I, and Supplementary Data 1.

Position is a separate physical registration

Centring L0≈90.60 in gives equal 51.844° arms. Petrie's present transverse correction splits them by 3.62°; alternative clearance subsets give splits of 3.50–3.75°. The current state therefore fails robustly.

Under the R10.1 triple-register criterion, each lateral gap remains within 1% of D only for a centre displacement within +/-14.65 mm, a full accepted width of 29.30 mm. The present displacement of 245.1 mm is 16.7 times that semiwindow. The separately frozen exterior-angle protocol is stricter, with a central allowance of 0.09447 in. These thresholds answer different questions and are not combined. No surviving trace yet recovers the original position. Figure 4 summarises the positional registration and ablation.

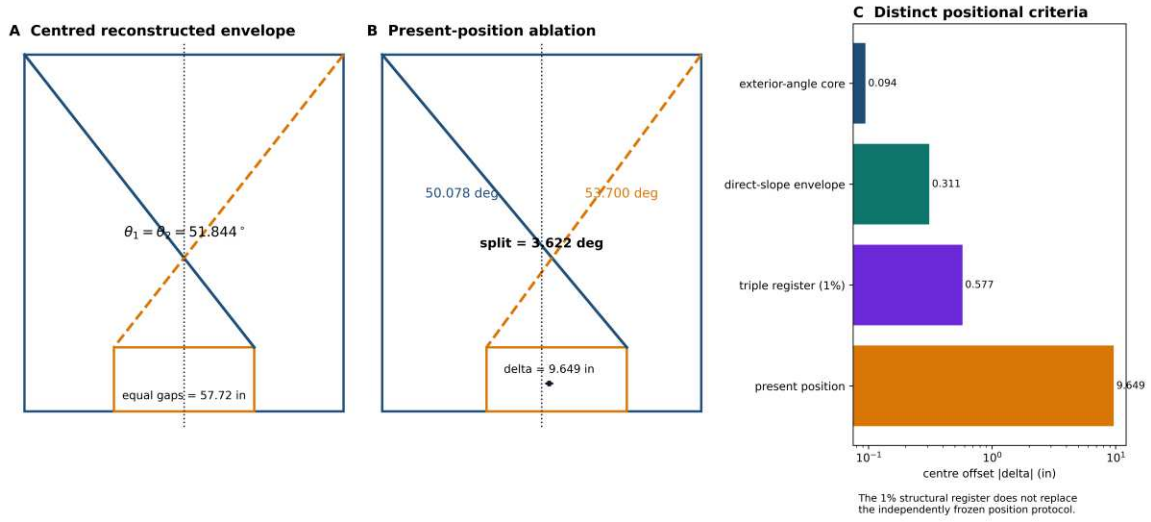


Figure 4. Position registration. (A) Centred L0=90.60 in gives equal 51.844° arms. (B) Present correction splits them by 3.622°. Geometric aspect is equal. (C) Frozen angle, slope and triple-register bands and present offset use a logarithmic scale; thresholds answer different questions. Source: authors' calculations.

Vertical registration and survey identifiability

The decoder depends on the ceiling-to-coffer-top clearance G, not on an arbitrary coordinate origin. If z is the physical coffer-base elevation above the chosen floor datum, G=H−h−z. Raising the coffer changes G; translating the common coordinate origin changes neither G nor the profile. Near the primary dimensions, a 1-mm change in W changes L by +0.737 mm, while a 1-mm change in H, h or z changes L by −0.324, +0.324 or +0.324 mm, respectively. Geometry alone identifies the combined clearance and cannot

separately recover changes in H, h and z. This distinction defines the vertical observations needed in a new survey.

Body top and lid surface define distinct geometric states

The primary relation uses the coffer-body top. A level lid seated flush in the 1.70-in ledge leaves L unchanged. With other inputs fixed, the 0.2% length criterion allows its surface from 19.44 mm below to 8.97 mm above that top; a hypothetical 3-in lid exceeds the criterion. This defines the scope of a lid-surface construction, without excluding a historical lid or the body-top relation. Effective-thickness conventions, inversion and scenarios are in Supplementary Information, Part I, S24.

Comparative and functional controls

The Queen's Chamber finished gable rises at 30.501 degrees rather than the exterior face. Transferring the D=g decoder while retaining the Khufu sarcophagus height gives 42.412 degrees using the wall-top height and 54.407 degrees using the gable apex; neither reproduces the profile. These are operator-transfer tests, not homologous sarcophagus controls.

At Hawara, the transverse body section gives 27.363°, while D=g predicts 24.972° and a width of 64.27 in against the measured 48.4 in. The entire grammar yields no width match within 0.2% among 69 classes in the original domain or 131 in the proportional domain; the nearest class misses by 0.541%. For every positive coffer width, the body-section angle remains below 38.077°, below all three reported exterior fragments. This angular ceiling rules out recovery of Hawara's exterior slope by the construction; discrimination within the transferred grammar therefore rests on measured width. Hawara's curved lid defines a separate state (Supplementary Information, Part I, S24).

Removing the supplementary ideal volume-balance hypothesis removes the R12 inverse and its R13 joint reconstruction, while leaving the D=g decoder, morphology-based validation, exterior-angle check, R10.1/R11 specificity, position test and Hawara control unchanged. The primary result therefore does not depend on the cavity-volume relation or an interpretation of the cavity's function. The downstream and comparative controls are summarised in Figure 5.

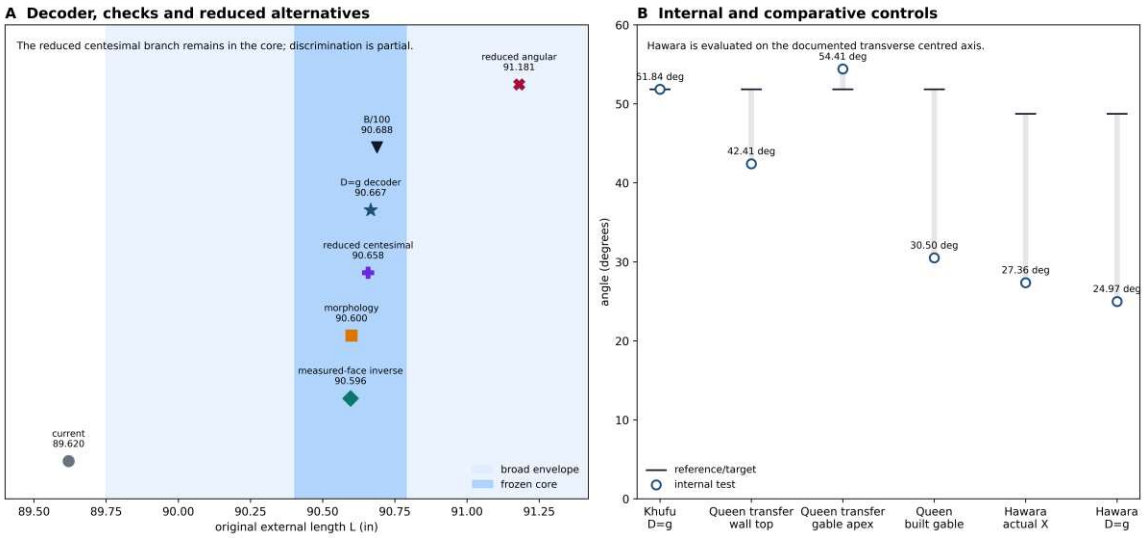


Figure 5. Downstream and comparative controls. The reduced angular branch lies outside the core but inside the broad envelope; the reduced centesimal branch stays in the core. Transverse Hawara gives actual X=27.36° and decoder=24.97°. Source: authors' calculations.

Discussion

The central result is that preserved interior dimensions reconstruct a damaged object and connect its envelope to the monument's exterior profile through one reversible relation. Under the centred D=g construction, A=(H−h)/W determines the missing length ratio r_Dg=L_Dg/W and its associated line direction; the reverse calculation gives the interior proportion required by a specified exterior profile. The sarcophagus, chamber and pyramid can therefore be examined as a coupled geometric system. This is the operational meaning of dimensional encoding in this study.

The construction also explains why several familiar proportions appear together. Under D=g, r=11/25 produces the partition 7|11|7; introducing the external scale B/W≈44 gives B/L≈100. Figure 1 expresses these relationships as two opposed similar profiles, approximately 1:44 and 1:100 of the exterior, sharing a single apex. Their architectural interest is economy: one internal constraint organises several relationships and allows reconstruction in both directions. Because they follow from shared geometry, these manifestations receive no separate statistical weight.

Floor intercepts and nested subdivisions make the common line direction visible but introduce no additional constraint. Likewise, producing a length and an angle does not automatically supply two independent tests. In the declared rule comparison, length alone selects D=g and the tangent criterion adds no rejection. The visual coherence of the construction and its statistical discrimination must therefore be assessed separately.

Architectural context becomes a source of dimensional information for the lost envelope. The relation uses chamber width and the clearance above the sarcophagus, so end damage leaves the quantities required for length reconstruction available. Its application commits to identifiable physical corners and a restricted transverse placement. Those commitments connect the calculated envelope to traces that can be examined in the surviving object and room. Rule specificity, bounded-input stability and the altered-state controls quantify the support for this reconstruction.

The relation is especially informative because different disturbances produce different signatures. Longitudinal damage changes L while W, H and h remain available for reconstruction. Transverse displacement breaks g_N=g_S and separates the two arms. A physical change in the vertical clearance alters A and the recovered profile. The model thus connects geometry to three different material questions rather than absorbing every discrepancy into one adjustable dimension. For heritage documentation, this separation identifies what a new observation would actually test.

The historical volume check gives L_V=90.58 in, 0.41 mm from morphology and 2.10 mm from D=g. The two calculated lengths bracket the morphological estimate. Because they share coffer measurements and the volume route assumes ideal balance, these comparisons form one linked consistency check.

The joint reconstruction makes external height an output of the two relations and recovers both dimensions of the same damaged object when h is no longer supplied. R14 compares rules under a common volume condition and retains D=g as the sole length match among 154 classes. The persistence of the selected relation across the supplied-height and reconstructed-height formulations extends the reconstruction from one dimension to a coupled envelope.

The seven-route audit does not rank D=g first by central length agreement. The ideal-volume route is closer, and proportional alternatives also lie nearby. Their assumptions and inputs differ (Supplementary Information, Part I, Table S14). D=g is distinguished by its physical-segment equality, specificity within the declared grammar and material consequences; central residual alone cannot select historical design.

The decoder neither erases nor simply duplicates Petrie's observations. The approximate relation h/W≈1/5 is a previously published vertical proportion, and shared cubit metrology provides an alternative explanation for B/W≈44 considered alone. The contribution is the reversible mapping between those interior measurements, the damaged envelope and the profile, together with explicit tests of its physical registration.

Relative to the ideal A=252/275, measured A differs by 0.0146%, whereas Petrie's reduced composition $\sqrt{5}/2-1/5$ differs by 0.1823% and predicts L≈90.546 in under D=g, about 3.06 mm from the measured-input decoder. The reduced baseline explains much of this numerical neighbourhood without selecting the crossed endpoints, imposing D=g, requiring transverse centring or evaluating the damaged envelope separately. Those additional commitments distinguish the constructions structurally. R10.1 quantifies specificity within the declared grammar; historical survey bounds still limit full-model discrimination between the measured and reduced constructions.

For heritage reconstruction, the useful outcome is an explicit connection between a proposed form and observations that could reject it. The present relation complements computational hypothesis testing at Giza [7] by addressing the sarcophagus envelope and its placement. It uses metrological closure rather than the equilibrium constraint of Meriggi et al. [8], while sharing with uncertainty analysis [9] and reconstruction from historical documentation [10] the need to distinguish evidence from assumptions. None of these approaches makes a computed arrangement an observed original state.

Historical reviews document incompatible pyramid interpretations [14,16], and Markowsky [17] illustrates the flexibility of numerical correspondences when candidate dimensions proliferate. The present model answers that methodological problem by declaring inputs, alternatives and rejection conditions. Its contribution is this reproducible combination of tests for a specific coupling; the study does not systematically rank all mathematical interpretations of Khufu or claim uniqueness beyond its declared grammar.

The relation was identified from historical measurements. Its physical roles, comparison family and selection therefore require explicit scrutiny, which the declared grammar and controls make reproducible. Independent surveys provide the next material test of the proposed reconstruction.

The largest limitation is L0. Petrie's approximately 90.60-in reconstruction derives from damaged curvature and straight-edge comparison and lacks a modern uncertainty distribution. Agreement at hundredths or thousandths of an inch must therefore be read as central-value closure. A high-resolution scan should reconstruct the ends without receiving any geometric target.

The original transverse position is also unknown. The present sarcophagus is displaced, tilted and lifted; no placement line has been recovered. Centring is therefore a geometric requirement of the proposed symmetric construction and a prospectively testable historical hypothesis, not a demonstrated original design decision or an observed original state.

R10.1 establishes one qualifying class within the declared grammar. The count 1/127 describes rule specificity; Panel 2 separately measures target frequency under the stated uniform plausible-ratio domains. The tangent criterion leaves the length-selected set unchanged. The comparative corpus remains small because each eligible monument requires a measured exterior, flat physical endpoints, a sarcophagus and adequate source provenance. R17 confirms the central ranking in both enlarged coefficient budgets and the leading rank across all 9,261 original-grammar input scenarios; S25 quantifies how qualifying alternatives and ranking stability change as the search expands (Supplementary Information, Part I).

Volume equality is an idealised historical criterion, explicitly inexact in Petrie's surviving measurements. Rectilinear restoration need not describe actual damage. Volume-domain frequencies remain sensitivities and share the coffer record.

The figures were regenerated with equal data aspect for every geometric panel. Pixel slope is nevertheless illustrative; the values in the text and data files are calculated from coordinates, not measured from rendered images.

Smyth's W=206.3 in, H=230.1 in and coffer h=41.27 in [18] give L=90.84 in, a +6.15-mm residual (0.267%), exceeding the 0.2% criterion. The angular residual of −144 arcsec also exceeds Petrie's ±65-arcsec band. This source substitution does not reproduce the primary agreements. Width dominates the numerical change, but endpoint and floor-datum equivalence are unresolved; the historical cause is not established. Smyth's conjectural height correction also exceeds both criteria. Original readings and exact decomposition are in Supplementary Information, Part I, S23.

Two blinded protocols remain decisive. Protocol A estimates the maximum original longitudinal envelope from the stone morphology alone. Protocol B estimates the original transverse centre offset from floor contact traces, wear, residue or archival coordinates. Analysts lock reports, exclusions, code and hashes before receiving predictions and decision bands.

Protocol A compares the decoder's 90.67-in prediction with measured-face inversion, historical volume balance, B/100 and reduced alternatives, retaining their full-precision values in Supplementary Information, Part I, and Supplementary Data 1. A future morphometric interval determines discrimination. Recovery of original centring tests material realization rather than another proportion.

A new survey should independently reconstruct the damaged end surfaces, investigate the original transverse position and record ceiling, coffer-top and base elevations in one vertical frame. Each

observation tests a different part of the relation. Accuracy assessment must accompany the three-dimensional record, as illustrated by Liu and Bin Mamat's heritage point-cloud study [19]; an instrument's nominal precision alone would not quantify uncertainty in an inferred missing surface. The recent King's Chamber ultrasound and inner-chamber material studies [5,6] supply relevant documentation context, but the morphometric and placement tests specified here have not been performed.

The broader contribution is a way to recover lost dimensions from relationships that survive elsewhere in an architectural ensemble. The Khufu case shows how to turn that possibility into an explicit reconstruction: define the physical endpoints, derive the missing quantity from preserved measurements, and assess the result against morphology, external geometry and competing rules. This approach can guide reconstruction where a documented geometric relationship links an incomplete component to its setting; D=g supplies the specific relation tested here.

Under the centred D=g construction, three preserved interior dimensions recover a 2.303-m sarcophagus envelope and a 51.838° profile, closely matching Petrie's historical comparisons without using the damaged length, exterior inclination or base as inputs. Information about the missing envelope remains recoverable through its geometric relationship with the chamber, while the same relation connects that reconstruction to the exterior pyramid. This gives the sarcophagus a testable role within the monument's spatial organisation and defines concrete targets for independent recovery of its original form and position.

Data availability

All numerical inputs and source attributions required to reproduce the analyses are included in Supplementary Data 1. The archive contains the historical measurements, frozen specifications, complete numerical outputs and machine-readable protocol thresholds. Supplementary Information contains the supporting derivations and tables (Part I), frozen envelope protocol (Part II) and frozen original-position protocol (Part III). The original historical survey publications are identified in the references. No new field measurements or scans were acquired for this study.

Code availability

All analysis code is supplied in Supplementary Data 1, including R01–R17, dependency requirements, execution instructions, stored outputs and SHA-256 checksums. The Python calculations require NumPy, pandas and SciPy; no external dataset download or repository access is required once dependencies are installed. The archive distinguishes the preserved R01–R16 code and frozen protocols, the exploratory R17 extension, and packaging and verification records. Optional figure-regeneration requirements are listed separately.

Acknowledgements

The authors thank the Grupo de Estudos Ágora for discussion and critical feedback. This research received no external funding.

Author contributions

L.G.R. conceived the study and performed the investigation, reverse engineering, geometric modelling, data curation and visualisation, and wrote the original draft. M.A.S. performed validation, critical analysis

and methodology review, and reviewed and edited the manuscript. Both authors approved the final manuscript and take responsibility for the work.

Competing interests

The authors declare no competing interests.

Use of artificial intelligence

The authors conceived and directed the study and take full responsibility for its methods, results and conclusions. OpenAI ChatGPT assisted with language editing, code drafting and reproducibility checks under author review.

References

1. Morishima, K. et al. Discovery of a big void in Khufu's Pyramid by observation of cosmic-ray muons. Nature 552, 386–390 (2017). https://doi.org/10.1038/nature24647.

2. Petrie, W. M. F. The Pyramids and Temples of Gizeh (Field & Tuer, 1883).

3. Procureur, S. et al. Precise characterization of a corridor-shaped structure in Khufu's Pyramid by observation of cosmic-ray muons. Nat. Commun. 14, 1144 (2023). https://doi.org/10.1038/s41467-023-36351-0.

4. Schumacher, T. et al. Confirmation of the ScanPyramids North Face Corridor in the Great Pyramid of Giza using multi-modal image fusion from three non-destructive testing techniques. Sci. Rep. 15, 9275 (2025). https://doi.org/10.1038/s41598-025-91115-8.

5. Maier, B. et al. Investigation of the lower block rows in the King's Chamber of the Great Pyramid using ultrasonic testing with shear wave arrays. Sci. Rep. 16, 19035 (2026). https://doi.org/10.1038/s41598-026-54151-6.

6. Sessa, C. et al. Material characterization of stone surfaces in the inner chambers of the Khufu (Cheops) Pyramid: towards informed conservation strategies. Sci. Rep. 16, 12586 (2026). https://doi.org/10.1038/s41598-026-48805-8.

7. Rosell Roig, V. L. A computational framework for evaluating an edge-integrated, multi-ramp construction model of the Great Pyramid of Giza. npj Herit. Sci. 14, 142 (2026). https://doi.org/10.1038/s40494-026-02405-x.

8. Meriggi, P. et al. A geometry-driven structural method for supporting archaeological modelling in partially preserved historic constructions. Heritage 9, 297 (2026). https://doi.org/10.3390/heritage9080297.

9. Apollonio, F. I., Fallavollita, F., Foschi, R. & Smurra, R. Multi-feature uncertainty analysis for urban-scale hypothetical 3D reconstructions: Piazza delle Erbe case study. Heritage 7, 476–498 (2024). https://doi.org/10.3390/heritage7010023.

10. Vaienti, B., Apollonio, F. I. & Gaiani, M. Analysis of Leonardo da Vinci's architecture through parametric modeling: a method for the digital reconstruction of the centrally planned churches depicted in Ms. B. Heritage 3, 1124–1147 (2020). https://doi.org/10.3390/heritage3040063.

11. Cole, J. H. Determination of the Exact Size and Orientation of the Great Pyramid of Giza. Survey of Egypt Paper 39 (Government Press, 1925).

12. Nell, E. & Ruggles, C. The orientations of the Giza pyramids and associated structures. J. Hist. Astron. 45, 304–360 (2014). https://doi.org/10.1177/0021828614533065.

13. Robins, G. & Shute, C. C. D. Mathematical bases of ancient Egyptian architecture and graphic art. Hist. Math. 12, 107–122 (1985). https://doi.org/10.1016/0315-0860(85)90002-3.

14. Rossi, C. Architecture and Mathematics in Ancient Egypt (Cambridge University Press, 2004). https://doi.org/10.1017/CBO9780511550720.

15. Petrie, W. M. F. Kahun, Gurob, and Hawara (Kegan Paul, Trench, Trübner, 1890).

16. Herz-Fischler, R. The Shape of the Great Pyramid (Wilfrid Laurier University Press, 2000). https://doi.org/10.51644/9780889207769.

17. Markowsky, G. Misconceptions about the golden ratio. Coll. Math. J. 23, 2–19 (1992). https://doi.org/10.1080/07468342.1992.11973428.

18. Smyth, C. P. Life and Work at the Great Pyramid during the Months of January, February, March, and April, A.D. 1865, Vol. II, 101–102, 119 (Edmonston and Douglas, 1867).

19. Liu, S. & Bin Mamat, M. J. Application of 3D laser scanning technology for mapping and accuracy assessment of the point cloud model for the Great Achievement Palace heritage building. Herit. Sci. 12, 153 (2024). https://doi.org/10.1186/s40494-024-01252-y.

Supplementary Files

This is a list of supplementary files associated with this preprint. Click to download.

- 03SupplementaryInformation.pdf
- 04SupplementaryData1.zip